ROBERT GORDON
UNIVERSITY ABERDEEN

OpenAIR@RGU

The Open Access Institutional Repository at Robert Gordon University

http://openair.rgu.ac.uk

This is an author produced version of a paper published in

Composite Structures (ISSN 0263-8223)

This version may not include final proof corrections and does not include published layout or pagination.

Citation Details

Citation for the version of the work held in 'OpenAIR@RGU':

NWOGU, N. C., KAJAMA, M. and GOBINA, E., 2015. A study of gas diffusion characteristics on a micro porous composite silica ceramic membrane. Available from *OpenAIR@RGU*. [online]. Available from: http://openair.rgu.ac.uk

Citation for the publisher's version:

NWOGU, N. C., KAJAMA, M. and GOBINA, E., 2015. A study of gas diffusion characteristics on a micro porous composite silica ceramic membrane. Composite Structures, Vol. 134, pp. 1044-1050.

A study of gas diffusion characteristics on a micro porous composite silica ceramic membrane

Ngozi Claribelle Nwogu, Mohammed Kajama and Edward Gobina*

Centre for Process Integration and Membrane Technology, School of Engineering, the Robert Gordon University, Aberdeen. United Kingdom.
*Corresponding Author: E-mail: e.gobina@rgu.ac.uk. Phone No.: +44(0)1224262309.

Abstract

The purpose of this study is to investigate gas permeation behaviour of five gases (CO_2, He, H_2, N_2 and Ar) across two silica modified ceramic membranes, Membrane Y and Membrane Z. An examination of the variations in their layer thickness and flow rate was determined. Solution-dip coating process was used for the modification process specifically for pore size reduction. This resulted in some level of modifications in the layer thickness after a successive dipping time as well as flow rate in relation to pressure drop. The effect of number of dips generally influenced the layer thickness of both membranes. Membrane Y layer thickness through five successive dipping was in the range of 89.2-36μm while Membrane Z ranges between 150.72-43.69 μm. Gas permeability as a function of mean pressure for membrane Z was calculated using data obtained experimentally. The permeation tests confirmed the contribution of both Knudsen and viscous flow mechanism with an estimation and prediction of the membrane pore radius.

Keywords: Ceramic membrane, gas diffusion, dip-coating, Knudsen flow & viscous flow

1. Introduction

Gas separation process through membrane technology has so far demonstrated good prospects and great advantages over conventional technologies. Generally, membranes are channels for mass transfer of gas molecules in gas separations [1] [2] [3]. Inorganic ceramic membranes have a broad spectrum of application at industrial level as a result of their ability to give excellent performance under harsh operating state/condition, high mechanical strength, high chemical stability, easy cleaning, high resistance to acidic chemicals and the ability to withstand high pressure and temperature especially in CO_2 capture applications [4] [5]. Some areas of its application are in gas purification, ultra filtration processes and treatment of waste water. Inorganic membranes can further be classified as porous or non-porous. While non-porous inorganic membrane is made up of dense separation-film resulting in very good selectivity and minimal permeance, porous type of membrane have lower selectivity and high permeance with pore sizes of up to 10μm [6]. Porous membranes have micro-pores that allow the passage of fluid through its channel while dense or non-porous membranes, allow the flow of fluids to take place through the bulk membrane material itself. Diffusion of fluid is as a result of pressure or concentration gradient [7]. However, ceramic membrane forms the main class of inorganic membranes consisting of three basic types and pore sizes- macro porous (> 500Å), meso porous (500-20 Å) and micro porous (<20 Å). Gas permeation across a porous ceramic membrane with a thin layer is influenced by three factors namely the gas properties, morphology of the membrane and the material used for membrane design [8]. Therefore the membrane layer thickness, porosity of the membrane surface, pore size and its distribution are some parameters in the membrane structure which determines the performance and efficiency of the membrane for gas separation and purification purposes [9] [10]. Membrane morphological characterization can be achieved through some notable methods such as scanning electron microscope (SEM), bubble point technique, mercury porosimetry and Nitrogen gas adsorption-desorption [9] [11] . In essence gas transport through porous ceramic membrane pores can be obtained based on the kinetic theory of gases. Different transport mechanisms exist and in doing so an assumption that the membrane pores are a package of tubes can be made [1]. In addition, depending on the pore size of the membrane, these mechanisms can be theoretically characterized by permeability through the porous membrane [12] [13]. Three main types of mechanisms that are generally involved for mass transfer through porous media are Knudsen flow, slip flow and viscous flow. Others are surface diffusion and molecular sieving. The mean pore radius and the mean free path of the gas molecules are two factors in transport mechanisms and are represented by r_p and λ respectively. Accordingly, the mean free path is the average distance travelled by the molecules between collisions. Further, when the ratio of membrane pore radius to that of mean free path is less than 0.05, Knudsen flow is prevalent. Between the ratio of 0.05 and 3 is described as slip flow while for a ratio above 3 viscous flows is applicable [14] [1]. In Knudsen diffusion the flow takes place when the pore diameter is smaller than the mean free path of the diffusing gas molecules i.e. $r_p < \lambda$. With low density, the gas molecules collide with the walls more frequently than with each other. It is distinguished by a Knudsen number, which is a measure of the relative

importance of Knudsen diffusion. The flux due to Knudsen flow is inversely proportional to the square root of the molecular weight of the gas permeating through the membrane, the higher the molecular weight the lower the molecular velocity of the gas. Better separation and less permeation are more characteristic features present in Knudsen flow and flow occurs mostly in micro porous and meso porous membranes [15].

Flux due to Knudsen mechanism is generally expressed by equation (1) [15];

$$F_K = \frac{8_{rp}}{3(2\pi MRT)^{\frac{1}{2}}}$$
(1)

Where F_K is the gas flux due to Knudsen diffusion, r_p, membrane pore radius (m), M molecular weight of the permeating gas (kg/mol), R gas constant (J/mol.K) and T temperature (K)

In viscous flow regime, the distance between gas molecules are smaller compared to the transverse channel. Subsequently the main driving force in viscous flow mechanism is molecule to molecule collusions, minimal interaction with the pore walls, high permeability and little or no separation is achieved since the viscosities of gases are very close to each other ie $r_p > \lambda$. According to Hagen poiseuille formula, flow due to viscous is determined by equation (2) [15] [16].

$$F_V = \frac{rp^2}{8\mu RT} \frac{[P_1 + P_2]}{2}$$
(2)

Where F_V is gas flux due to viscous flow, μ is the gas viscosity (µpas), P_1 and P_2 are absolute and atmospheric pressure (bar) respectively. The diagram in figure 1 shows a typical disparity between Knudsen and viscous flow transport mechanism.
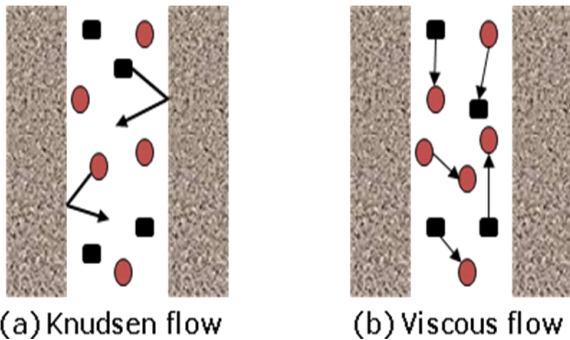

(a) Knudsen flow   (b) Viscous flow

Figure 1: Difference in flow Pattern between Knudsen and Viscous transport mechanism [17].

Aluminium oxide (Al_2O_3), Titanium Oxide (TiO_2), Zirconium Oxide (ZrO_2), Silicon dioxide (SiO_2), Silicon carbide, Zeolite or a hybrid mixture of two or more materials of their oxides can be used for the fabrication of composite ceramic membranes. Design of the membrane can employ the use of sol gel technique which modifies the pore size of membrane with high level superficial area through dip coating process [7] [18] [19] [20] . Some advantages of sol gel technique as reported by several authors includes a nanometre scale pore size distribution, homogenous pore size distribution and fabrication of a top layer capable of a comprehensive pore size control[18] [21] [22]. One major complexity encountered during membrane fabrication is on how to tackle the relationship between getting high flux and high selectivity materials. This can be attributed to the inverse proportionality of flow rate to membrane layer thickness [6] [23]. Some other researchers [23] in their study looked at the relationship between membrane structure and permeation with respect to the material make up of the membrane. An estimation of permeability due to viscous flow can be achieved theoretically and experimentally, gas permeability due to Knudsen flow can be predicted using simulation techniques. In this present study, single gas permeation through two different micro porous composite ceramic membranes is investigated. Permeability due to both viscous and Knudsen flow mechanisms are obtained through theoretical calculations and experimentally. In addition the relationship between the membrane pore size and membrane layer thickness as a function of pressure drop is also investigated.

1.1 Basic mathematical equations of mass transfer through a porous medium

The simplest generally applied mathematical equation to describe transport of gas molecule components through a porous medium is characterized by Knudsen and viscous flow. Therefore the total flux across the membrane is calculated by combining equation I and 2 above [15] [16].

$$F_{total} = \frac{8_{rp}}{3(2\pi MRT)^{\frac{1}{2}}} + \frac{rp^2}{8\mu RT} \frac{[P_1 + P_2]}{2}$$
(3)

where F_{total} is the total flux through the membrane

Equation (3) can be rearranged as;

$$F_{Total} = F_K + F_V P_{avg}$$
(4)

Where P_{avg} is the average pressure. To determine the permeability of a single gas across the membrane as a function of pressure drop and to be able to calculate the membrane pore radius, further rearrangement of equation 4 is illustrated below:

$$F_{total} = \frac{8_{rp}[P_1 - P_2]}{3(2\pi MRT)^{\frac{1}{2}}} + \frac{rp^2}{8\mu RT} \frac{[P_1^2 - P_2^2]}{2}$$
(5)

Equation (5) is obtained by manipulating equation (3)

To further obtain the actual equation for F_K and F_V taking into account the membrane layer thickness δ, equation (5) becomes

$$F_{total} * \frac{\delta}{(P_1 - P_2)} = \frac{8_{rp}[P_1 - P_2]}{3\delta(2\pi MRT)^{\frac{1}{2}}} * \frac{\delta}{(P_1 - P_2)}$$

$$+ \frac{rp^2(P_1 - P_2)(P_1 + P_2)}{16\delta\mu RT} * \frac{\delta}{(P_1 - P_2)} \tag{6}$$

Where

$$F_{total} * \frac{\delta}{(P_1 - P_2)}$$

= Permeability having its unit of measurement as molmm^{-2}s^{-1}pa^{-1} [15]

Equation (6) can further be simplified thus;

$$F_{total} * \frac{\delta}{(P_1 - P_2)} = \frac{8_{rp}}{3(2\pi MRT)^{\frac{1}{2}}} + \frac{rp^2}{8\mu RT}\left(\frac{P_1 + P_2}{2}\right) \tag{7}$$

In this paper, equation 7 will be used in determining parameters relating to the membrane structure. The permeability of all permeating species is also investigated.

2. Experimental methods

2.1 Membrane make up

Two ceramic membranes were selected for fabrication in gas diffusion and separation experiment, Membrane Y and Membrane Z. The two tubular inorganic ceramic membranes are designed by the use of commercially available supports (membrane support) from Ceramiques Techniques et Industrielles (CTI SA) France, with average pore diameter of 6000nm. The fresh supports are an assembly of 77% α-alumina and 23% TiO$_2$. The total effective and impermeable lengths of the supports are 318mm and 50mm respectively. However Membrane Y has an internal and outer diameter of 19.8 mm and 25 mm respectively while Membrane Z has 19.0 mm and 25 mm as its internal and outer diameter correspondingly.

2.2 Membrane modification

The modification process for both membrane supports involved the formation of a thin separating layer made up of silica fashioned through a successive dip coating technique. The silica solution consists of 900mls of 2-methylbutane, 100mls of silicon elastomer and curing agent. A mixture of the above stated quantity of Iso pentane, silicone elastomer and 10mls of curing agent which prevents a cross linking between silica molecules. The mixture was then poured into a large beaker and placed on a magnetic stirrer for 30mins until a clear solution was obtained. The entire mixture was

stirred continuously until complete homogeneity was achieved. The final solution was then poured into a 1000mls graduated cylinder. The solution preparation was carried out in the laboratory under a patented innovation from a renowned researcher [7] [8]. For Membrane Y, immersion in the silica-based solution was performed five times before gas permeation. Membrane Z was modified five times with gas permeation carried out after each dip. The different methods applied during the dip- coating resulted in variations of the membranes structural make up as well as their thicknesses. The silica solution used for Membrane Y had a higher concentration compared to that for Membrane Z. This is because additional chemicals were not required since permeation test was only carried out after the fifth dip, while for Membrane Z about 50mls of Iso-pentane was added to the solution to boost the concentration and rate of solution penetration through the membrane pore network. An initial drying method was applied through a spinning device for 30mins during the entire process with further drying in an oven at a temperature of 65°C for a period of 2hrs. The weight of the membrane supports before and after modification was obtained. An estimation of the mass gained and the layer thickness of the membrane after each dip was calculated using formula below:

$$\frac{W_{gain}}{\rho_{silicon} * A_S} \tag{8}$$

where $\rho_{silicon}$ is the density of silicon (2.1g/cm^3), A_S is the surface area of the support's outside surface and W_{gain} the weight gain by support after each dip.

2.3 Gas permeation test

The gas flow system however comprises of three main sections, namely: the feed delivery, the permeator and flow measurement. The gas permeation test was carried out at room temperature using 5 single gases, namely: H$_2$, N$_2$, Ar, CO$_2$ and He. A schematic diagram of the experimental set up is shown in figure 2 and consists of tubular membrane reactor which houses the ceramic modified membrane, a gas inlet flow line through which gases are introduced into the ceramic membrane and a digital mass flow meter used to measure the rates during the permeation test while maintaining a particular pressure drop across the membrane. Characterization of the membrane by scanning electron microscopy as well as the elemental composition using energy dispersive x-ray analysis was also obtained.
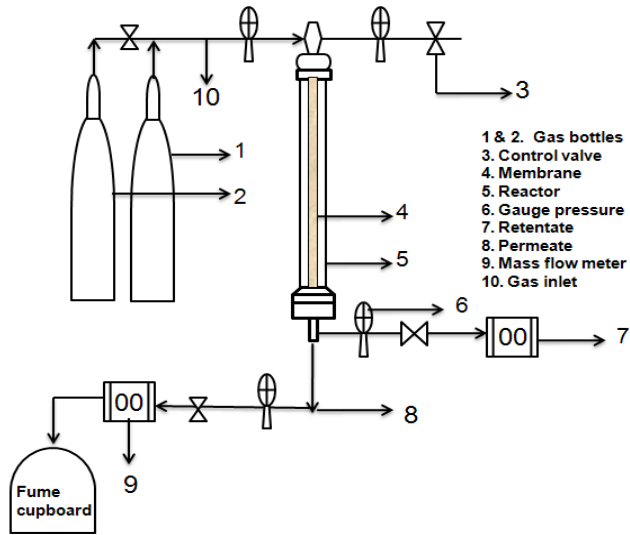
Figure 2: conceptualized diagram of the experimental set up

2.4. Characterization of the membrane

The elemental composition of the membrane support comprises of TiO_2 and Al_2O_3. After the modification process, SiO_2 was added to the other elements already present in the membrane. Figure 3 and figure 4 depicts the SEM of the unmodified and the modified membrane respectively [24] showing a clear distinction between both images. An analysis of the adsorption and desorption curves for surface area estimation from the nitrogen adsorption isotherms is presented in figure 5 and Table I.
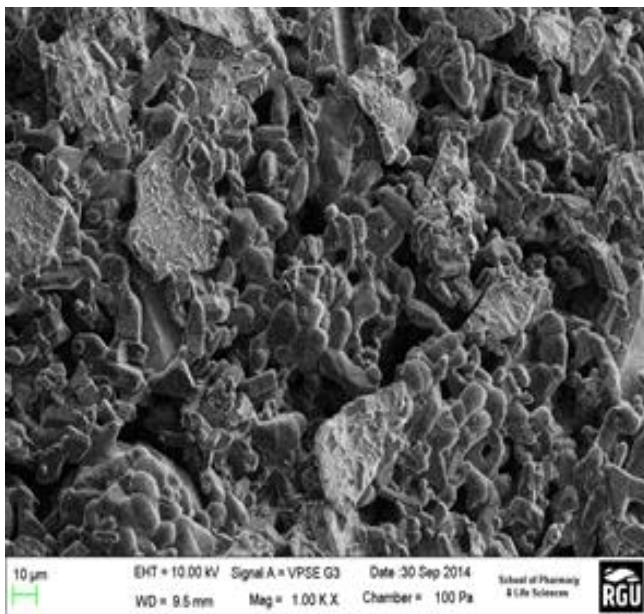

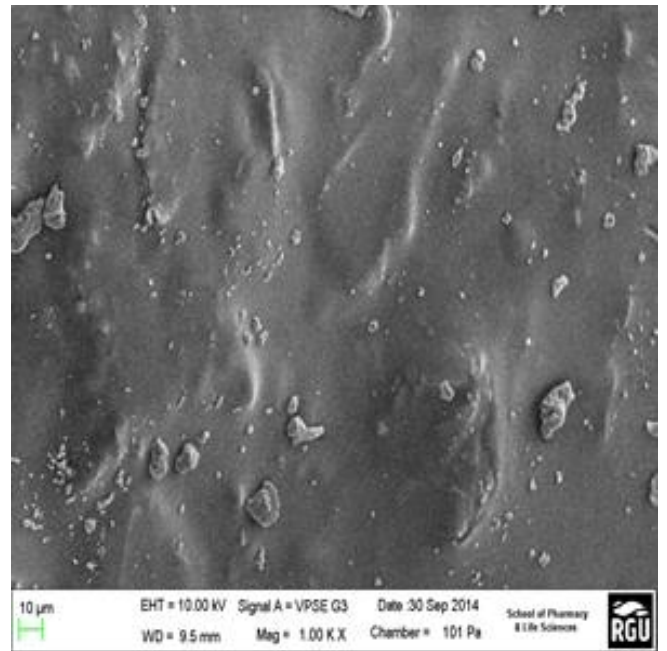**Figure 3: SEM micrograph ceramic support with 1.00kx magnification**

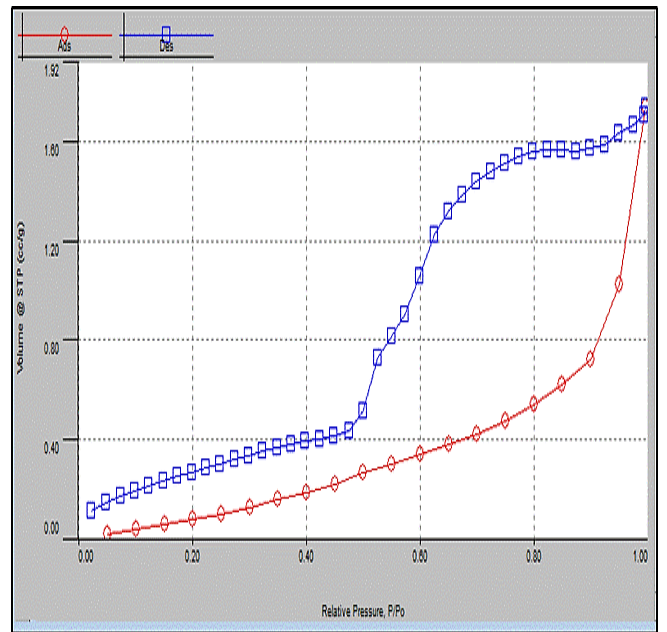**Figure 4: SEM micrograph modified ceramic**

Figure 5: Linear Isotherm of Gas Adsorption and Desorption

Table 1: BET CURVE SUMMARY

BET SUMMARY	
Slope	782.459
Intercept	2.48E+03
Correlation coefficient,r	1
C constant	1.316
Surface Area	1.068

3. Results and discussions

3.1. Effect of dip-coating on membrane layer thickness

The weight of the ceramic support was calculated before and after each dipping during the dip-coating process. This was done to ensure that concise and accurate thicknesses of both membranes could be estimated. Table 2 and 3 gives the calculated average thicknesses of Membrane Y and Membrane Z. The membrane surface area of membrane Y and membrane Z are $0.025m^2$ and $0.022m^2$ respectively. The cross-sectional structure of the membrane could not be obtained as this would entail breaking the membrane into smaller pieces and taking the X-section. However, witness samples were used to obtain SEM of the X-section.

Table 2: Calculated membrane layer thickness for Membrane Y after each dip

	Membrane Y	
Dip	Thickness (μm)	Thickness (m)
1	89.2	8.92E-05
2	62.6	6.26E-05
3	49.3	4.93E-05
4	43.6	4.36E-05
5	36.0	3.60E-05

Table 3: Calculated membrane layer thickness for Membrane Z after each dip

Membrane Z		
Dip	Thickness (μm)	Thickness (m)
1	150.72	15.0E-05
2	91.74	9.17E-05
3	87.37	8.74E-05
4	54.61	5.46E-05
5	43.69	4.37E-05

As observed in Tables 2 and Tables 3, the values of the layer thicknesses of both membranes vary with Membrane Z having higher layer thickness than Membrane Y. This is attributed to the different methods used during the dip coating. The silica solution used for membrane Z stayed longer on the magnetic stirrer and gas permeation was carried out after each dip. As a result the tendency of a decrease or loss in the concentration of the solution occur leading to addition of more elastomer. This enhanced both the concentration and penetration rate of the solution. However for Membrane Y, gas permeation test was only conducted after the fifth dip-coating modification. In addition membranes were sealed before applying the dip-coating process on the outside surface to prevent the coating of inside of the membranes. Nonetheless a small amount of Iso-pentane was added just before the fifth dip.

3.2. Analysis of gas transport across two coated supports

Determination of gas flow rate as a function of pressure drop was investigated for both membranes. Figure 6 and Figure 7 are single gas permeation test conducted on membrane Y and Membrane Z. Results obtained from the plot show that the flow rate across Membrane Y exceeded that of Membrane Z. It is also important to note that the thickness of both membranes came into play. As shown earlier in tables' 2 and 3, the layer thickness of Membrane Y is less than that of Membrane Z. This is a clear indication that the higher the thickness the more the resistance, hence layer thickness affects gas permeation in the entire process. Again for both membranes, the flow rate of gases has a linear proportionality with pressure drop.

Furthermore, for the flow rate of gases through membrane Y, notice that CO_2 gas had the lowest flow rate as expected due to its high molecular weight of 44. He gas with a molecular weight of 4 permeates faster than all the gases. H_2 flow rate was lower than that of He even though it had a lower molecular weight. This could be explained in terms of the kinetic diameter of He (2.65Å) which is lower than that of H_2 (2.89 Å). The trend of the gas flow obviously is not dominated by Knudsen flow except for that of CO_2. An estimation of the statistical error represented as error bars is shown in figures 6a and 7a.
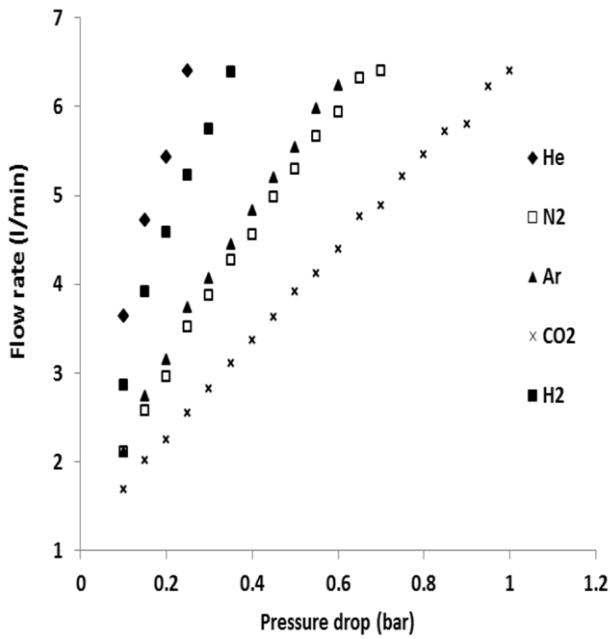
Figure 6: Single gas permeation at room temperature (25ºC) for Membrane Y after 5th Dip Coating
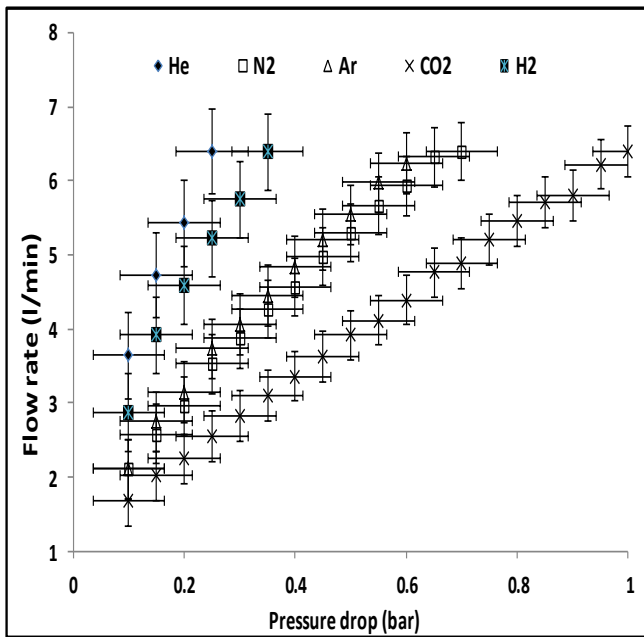

Figure 7: Single gas permeation at room temperature (25ºC) for Membrane Z after 5th Dip Coating

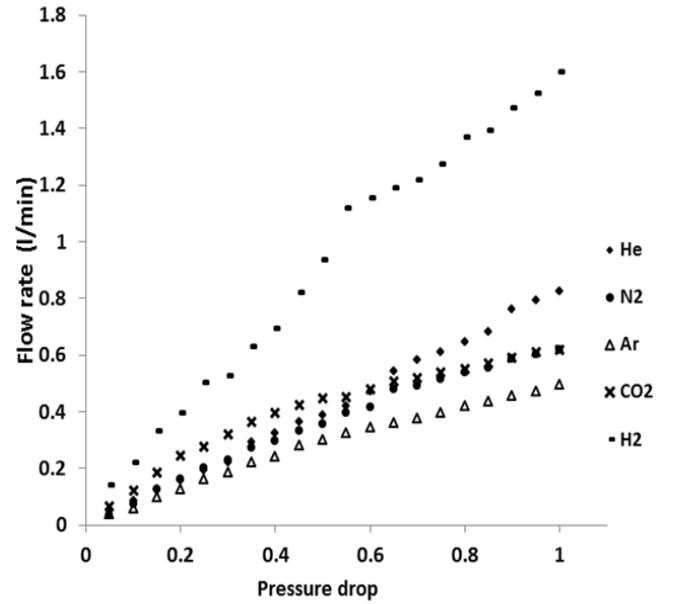**Figure 6a: Estimation of statistical error for single gas permeation (25ºC) of Membrane Y after 5th Dip Coating**
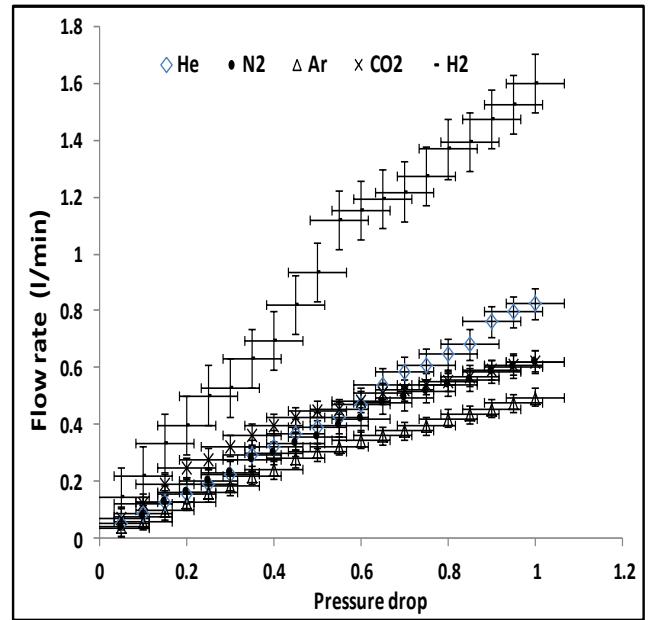

Figure 7a: Estimation of statistical error for single gas permeation (25ºC) of Membrane Z after 5th Dip Coating

Gas permeation across membrane Z took another dimension. We observe that CO_2 gas with the highest molecular weight of 44 permeated faster than Ar and N_2 with molecular weight of 40 and 28 respectively. The possibility of surface diffusion mechanisms as a result of the modification can be used to explain the trend. However a different scenario applied for H_2 with the lowest molecular weight 2 as expected permeated a lot faster through Membrane Z showing a dominance of Knudsen mechanism in the flow. Consequently the flow rates of individual gas did not actually follow the order of their molecular weights for both membranes, although there is a clear indication that CO_2 gas

is a strongly adsorbing gas for Membrane Z than Membrane Y.

3.3. Permeability and mean pressure

The calculated thickness was used to obtain permeability values of the gases through Membrane Z which are then plotted against the mean pressure. Figure 8 is a graphical representation of permeability of the different gases through Membrane Z at room and different operating pressures (range 1.1- 1.5 bar). Notice from the graph that there is an obvious disparity between permeability trend line of H_2 and CO_2. It can be observed that as the mean pressure increases, the permeability for H_2 also increases. However, permeability decreased with mean pressure for CO_2.

However, there exists a possible viscous flow mechanism for H_2 permeability within the membrane network due to its high permeability values compared to other gases. Ar and N_2 gases displayed more constant permeability than CO_2 with mean pressure. An estimation of the statistical error represented as error bars is shown in figure 8a.
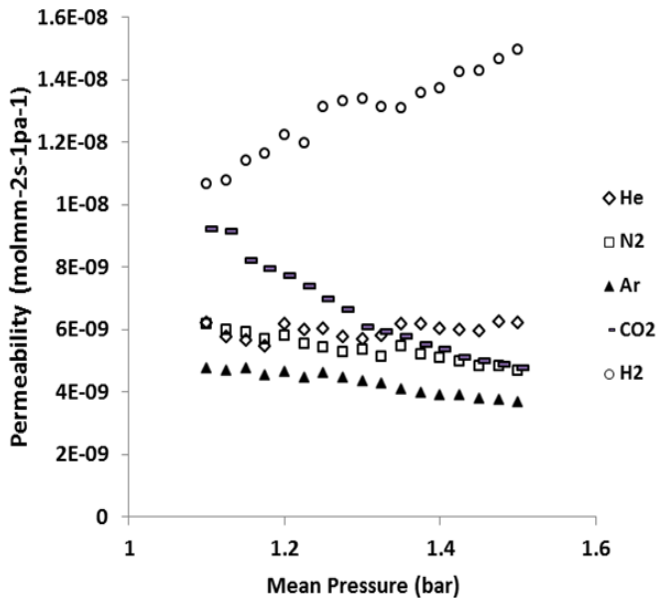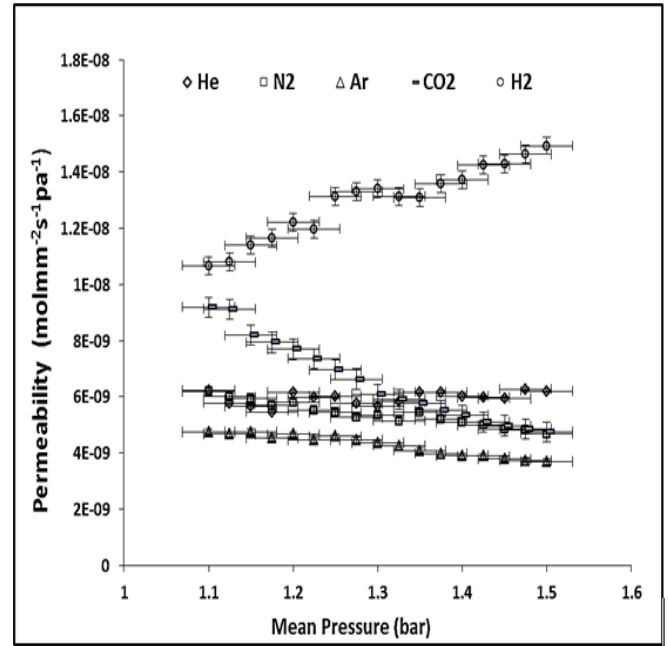

Figure 8a: Estimation of statistical error on the effect of mean pressure to permeability coefficient

3.4. Pore size prediction and estimation

As stated earlier, total flow of gas across a porous membrane could be achieved by different mechanisms. Subsequently, an estimate of an amount contributed by each mechanism can be determined from figure 9 showing the permeability trend line equation for CO_2 and H_2 gases. An estimation of the statistical error represented as error bars is shown in figure 7a. From equation 4, the slope is calculated with the formula below:

$$\frac{rp^2}{8\mu RT} \tag{9}$$

Similarly, intercept with the formula

$$\frac{8_{rp}}{3(2\pi MRT)^{\frac{1}{2}}} \tag{10}$$

By substituting H_2 and CO_2 permeability values from Figure 9 into equation (9) and (10) it is possible to estimate the pore radius (r_p). These are presented in Table 4. The values calculated are significantly lower than the pore size of the bare support. In addition, a macroporous membrane was obtained with a big difference between the first and second estimated pore radius. However, the pore size value from adsorption – desorption isotherm using the BET instrument could not be obtained at this time because in order to do so, the membrane would have to be destroyed. This cannot be done since the membrane is under evaluation for further studies.

Figure 8: Effect of mean pressure to permeability coefficient of different gases.

If you look at figure 9 used to estimate the pore sizes, the intercept in the case of H_2 is negative. So we have used the slope which is positive. Also, in the case of CO_2, the slope is negative so we have used the intercept. If Knudsen diffusion was the only transport mechanism in the membrane layer then permeability will remain constant as mean pressure increased. This is not the case for hydrogen which indicates viscous flow contribution. In the case of CO_2, the slope is negative which means that while viscous flow is assumed to be negligible, Knudsen flow is active but probably combined with surface flow. Surface flow is strongly governed by CO_2 adsorption and its mobility on the pore surface. In physical adsorption, the contribution of surface flow decreases with increasing temperature. Our experiments were carried out at room temperature which would indicate strong surface diffusion effect. There are numerous literature studies that show strong affinity of CO_2 in silica [12] [16] [24]. 'The pore size difference for H_2 and CO_2 shown in Table 4 can therefore be due to the calculations performed between the viscous flow and Knudsen flow. This is usual for such membranes to have a distribution of pore sizes. Since, permeability for Knudsen flow is directly proportional to the mean pore radius while permeability of viscous flow is directly proportional to the square of the mean pore radius. Work is currently undergoing to study the possible surface flow contribution in the case of CO_2 permeation though our membranes.
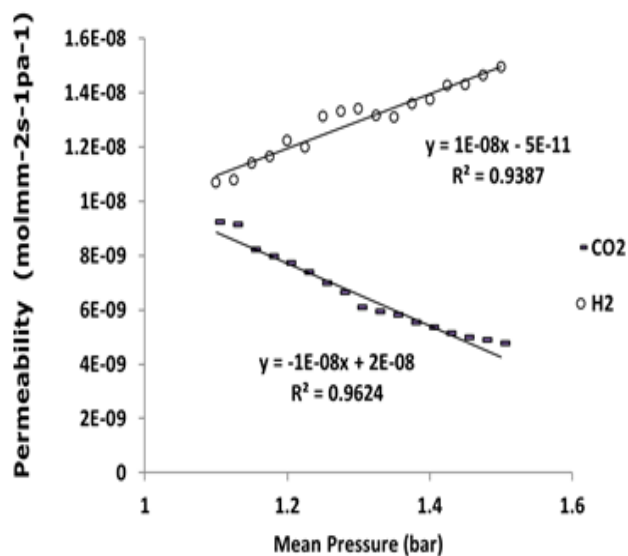

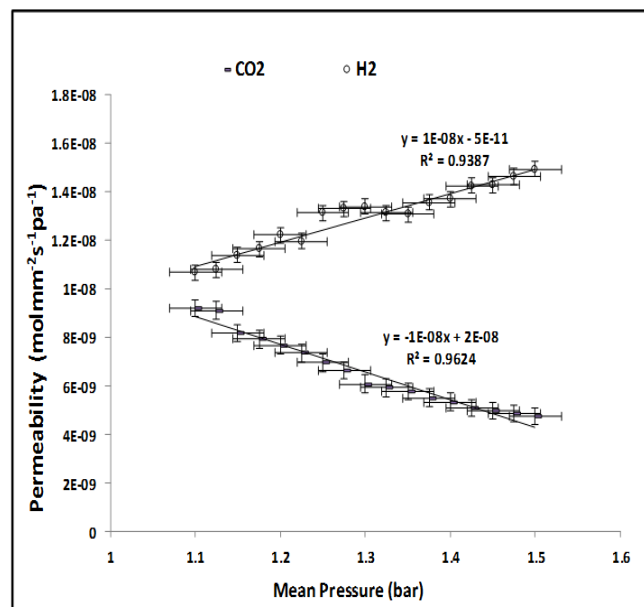**Figure 9: Pore size estimation through the effect of mean pressure on permeability coefficient of H_2 and CO_2 gases.**

Figure 9a: Statistical error estimation of mean pressure effect on the permeability of CO_2 & H_2 gases.

Table 4: Pore size estimation and prediction

Gas	Permeability coefficient $(molmm^{-2}s^{-1}pa^{-1})$	Estimated pore radius (m) x 10^{-5}
H_2	1	4.05
CO_2	2	0.16

4. Conclusion

Gas diffusion properties of two modified alumina ceramic membranes were investigated. Five gases CO_2, H_2, N_2, He and Ar were used for the permeation test. Overall results confirm that Membrane Z with higher thickness influenced the gases flow rate significantly by some measure of resistance in comparison to Membrane Y of smaller thickness. 'The single gas flow rate increases with an increase in pressure for both membranes. A comprehensive permeability determination of membrane Z confirms that the modification process resulted in conformal coverage. The significance of Knudsen and viscous flow mechanisms were beneficial and gave a better understanding of their individual contribution to the hydrodynamics of the membrane and pore size prediction.

Symbols

P_1	Absolute temperature (bar)
P_2	Atmospheric temperature (bar)
P_{avg}	Average pressure
R	Gas constant
F_k	Gas flux due to Knudsen diffusion

F_v	Gas flux due to viscous flow
A_s	Membrane surface area
M	Molecular weight of the permeating gas (kg/mol)
r_p	Pore radius (m)
T	Temperature (k)
F_{total}	Total flux through porous

Greek

λ	Mean free path
δ	Membrane layer thickness
μ	Gas viscosity (µpas)

Acknowledgment

References

[1] Huifeng Z.H.A.N.G. Mathematical Model of Gas Permeation Through PTFE Porous Membrane and the Effect of Membrane Pore Structure. *Journal of Chemical Engineering*. 2003; 11(4):383-387.

[2] Qi Z, Cussler E. Microporous hollow fibers for gas absorption: I. Mass transfer in the liquid. *Journal of Membrane Science.* 1985; 23(3):321-332.

[3] Qi Z, Cussler EL. Microporous hollow fibers for gas absorption : II. Mass transfer across the membrane. *Journal of Membrane Science.* 1985; 23(3):333-345.

[4] Li X, Liang B. Permeance of pure vapours in porous γ-Al2O3/α-Al2O3 ceramic membrane. *Journal of the Taiwan Institute of Chemical Engineers.* 2012; 43(3):339-346.

[5] Cheng Y, Pena M, Fierro J, Hui D, Yeung K. Performance of alumina, zeolite, palladium, Pd–Ag alloy membranes for hydrogen separation from Towngas mixture. *Journal of Membrane Science.* 2002; 204(1):329-340.

[6] Tüzün FN and Arçevik E. Pore Modification in Porous Ceramic Membranes With Sol-Gel Process and Determination of Gas Permeability and Selectivity. *Macromolecular symposia*: Wiley Online Library; 2010. p. 135-142.

[7] Kluiters S. Status review on membrane systems for hydrogen separation. *Energy Center of the Netherlands, Petten, The Netherlands.* 2004; .

[8] Ohwoka A, Ogbuke I, Gobina E. Performance of pure and mixed gas transport in reconfigured hybrid inorganic membranes Pt.2. *Membrane Technology.* 2012; 2012(7):7-9.

[9] Kong J, Li K. An improved gas permeation method for characterising and predicting the performance of microporous asymmetric hollow fibre membranes used in gas absorption. *Journal of Membrane Science.* 2001; 182(1):271-281.

[10] Shih H, Yeh Y, Yasuda H. Morphology of microporous poly (vinylidene fluoride) membranes studied by gas permeation and scanning electron microscopy. *Journal of Membrane Science.* 1990; 50(3):299-317.

[11] Porter MC. Handbook of industrial membrane technology. 1989; .

(12) Ohwoka A, Ogbuke I, Gobina E. Performance of pure and mixed gas transport in reconfigured hybrid inorganic membranes Pt. 1. *Membrane Technology.* 2012; 2012(6):7-12.

[13] Rao AB, Rubin ES. A technical, economic, and environmental assessment of amine-based CO2 capture technology for power plant greenhouse gas control. *Environmental science & technology.* 2002; 36(20):4467-4475.

[14] Ohlrogge K, Wind J and Brinkmann T. Membrane technology for natural gas processing. *SPE Gas Technology Symposium*: Society of Petroleum Engineers; 2002.

[15] Cui, Z. F., S. Chang, and A. G. Fane. The use of gas bubbling to enhance membrane processes. *Journal of Membrane Science* 221.1 (2003): 1-35. .

[16] Nwogu NC, Gobina E, Kajama MN. Improved Carbon Dioxide Capture Using Nanostructured Ceramic Membranes. *Low Carbon Economy.* 2013; 4:125.

[17] Benfer S, Arki P, Tomandl G. Ceramic membranes for filtration applications—preparation and characterization. *Advanced Engineering Materials.* 2004; 6(7):495-500.

[18] Benito J, Conesa A, Rubio F, Rodriguez M. Preparation and characterization of tubular ceramic membranes for treatment of oil emulsions. *Journal of the European Ceramic Society.* 2005; 25(11):1895-1903.

[19] Benito J, Conesa A, Rodríguez M. Membranas cerámicas. Tipos, métodos de obtención y caracterización. *Boletín de la Sociedad Española de Cerámica y Vidrio.* 2004; 43(5):829-842.

[20] Tsuru T. Inorganic porous membranes for liquid phase separation. *Separation & Purification Reviews.* 2001; 30(2):191-220.

[21] Burggraaf AJ, Cot L. Fundamentals of inorganic membrane science and technology. *Membrane Science and Technology.* 1996; 4(0)227-229

[22] Van Gestel T, Vandecasteele C, Buekenhoudt A, Dotremont C, Luyten J, Leysen R, et al. Alumina and titania multilayer membranes for nanofiltration: preparation, characterization and chemical stability. *Journal of Membrane Science.* 2002; 207(1):73-89.

[23] Kikkinides E, Stoitsas K, Zaspalis V, Burganos V. Simulation of structural and permeation properties of multi-layer ceramic membranes. *Journal of Membrane Science.* 2004; 243(1):133-141.

[24] Nwogu NC, Kajama MN, Dedekuma K, Gobina E. An Experimental Analysis of a Nano Structured Inorganic Ceramic Membrane for Carbon Capture Applications in Energy Security Challenges. *Energy and Environment Research.* 2014; 4(3):p1.